Direct Flow Visualization of Colloidal Gels in Microfluidic Channels

Mark T. Roberts,[†,§] Ali Mohraz,[†,‡] Kenneth T. Christensen,[⊥] and Jennifer A. Lewis*[,†,‡,§]

Frederick Seitz Materials Research Laboratory, Materials Science and Engineering Department, Chemical and Biomolecular Engineering Department, and Mechanical Science and Engineering Department, University of Illinois, Urbana, Illinois 61801

Received February 26, 2007. In Final Form: May 22, 2007

The behavior of colloidal gels under pressure-driven flow in square microchannels is quantified by microscopic particle image velocimetry (μPIV) and compared to predictions of available rheological models. The gels consist of hydrophobically modified silica microspheres ($\phi = 0.15-0.33$) suspended in a refractive index-matched fluid along with fluorescent tracers to aid visualization. Measured velocity flow profiles show a transition from plug flow to more fluid-like behavior with increasing volumetric flow rate (Q) at all ϕ. This transition is not captured by theoretical predictions of the flow profile based on the Herschel−Bulkley model. Rather, a model that accounts for gel breakup into a suspension of clusters at elevated shear rates by assuming a finite viscosity at infinite shear is needed to accurately predict the flow behavior of colloidal gels at large Q.

Introduction

Recent advances in the direct ink writing,[1−4] microextrusion,[5,6] and microfluidic assembly[7−9] of colloidal suspensions rely on their controlled flow through confined geometries, including fine nozzles, complex dies, and microchannels. In each of these approaches, phenomena such as shear thinning, wall slip, or jamming can lead to significant complications, especially at fine length scales (ca. $\leq 200\,\mu$m).[4,10,11] Moreover, the high shear rates involved can disrupt the particle network, leading to flow behavior that differs from that expected for colloidal gels.[12,13]

Rheological models have been developed to relate the deformation mechanics of viscoelastic materials to their material properties.[14−16] For example, the Herschel−Bulkley model is commonly used for colloidal gels to quantify the dependence of the shear rate on the applied shear stress:

$$\tau = \tau_y + K\dot{\gamma}^n \quad (1)$$

where τ is the shear stress, τ_y is the yield stress, $\dot{\gamma}$ is the shear rate, K is the power-law viscosity, and n is the shear-thinning exponent.[15] The parameters K, n, and τ_y can be obtained from rheological data for a given system. Coupled with equations of momentum and mass balance, eq 1 can then be used to predict the flow profile in a given geometry.[4,17−19] This model predicts that $\eta \to 0$ as $\dot{\gamma} \to \infty$, where η, the apparent viscosity, equals $\tau/\dot{\gamma}$. In contrast, theoretical and experimental studies of flocculation at elevated shear rates suggest that colloidal gels are broken down into a suspension of clusters that behave similarly to a colloidal fluid.[12,13] Break-up and reaggregation of these clusters result in a finite value of η. Therefore, the applicability of eq 1 at the large $\dot{\gamma}$ characteristic of those experienced during microchannel flow must be tested experimentally.

Visualization techniques, such as microscopic particle image velocimetry (μPIV),[20,21] confocal microscopy,[22] and nuclear magnetic resonance (NMR)[23] have been utilized to study the flow behavior of materials ranging from simple fluids to colloidal pastes. For example, μPIV has been used to study fluid flow within microchannels.[21] By incorporating fluorescent particles as flow-tracers, one can measure flow profiles with a spatial resolution approaching one micron at velocities up to 1 m/s. More recently, confocal microscopy has been employed to directly image the flow behavior of colloidal fluids ($\phi = 0.05-0.34$) in rectangular microchannels.[22] This technique is suitable for velocities up to ∼1 mm/s. At higher velocities, the particle images become considerably distorted. Finally, NMR has been used to investigate the flow profiles of concentrated colloidal pastes during ram extrusion.[23] This technique allows the internal flow of fluid relative to the colloidal network to be quantified along with the corresponding velocity profiles; however, a suitable velocity range was not reported.

Here, we employ μPIV to obtain flow profiles of colloidal gels in square microchannels. Using this technique, time-delayed pairs of images of fluorescent seed particles within a flowing

* Corresponding author.
† Frederick Seitz Materials Research Laboratory.
‡ Materials Science and Engineering Department.
§ Chemical and Biomolecular Engineering Department.
⊥ Mechanical Science and Engineering Department.

(1) Lewis, J. A. *J. Am. Ceram. Soc.* **2000**, *83*, 2341−2359.
(2) Lewis, J. A. *Curr. Opin. Solid State Mater. Sci.* **2002**, *6*, 245−250.
(3) Smay, J. E.; Gratson, G. M.; Lewis, J. A.; Shepherd, R. F.; Cesarano, J. *Adv. Mater.* **2002**, *14*, 1279−1283.
(4) Smay, J. E.; Cesarano, J.; Lewis, J. A. *Langmuir* **2002**, *18*, 5429−5437.
(5) Rao, R. B.; Krafick, K. L.; Morales, A. M.; Lewis, J. A. *Adv. Mater.* **2005**, *17*, 289−293.
(6) Wang, J.; Shaw, L. L.; Cameron, T. B. *J. Am. Ceram. Soc.* **2006**, *89*, 346−349.
(7) Terray, A.; Oakley, J.; Marr, D. W. M. *Science* **2002**, *296*, 1841−1844.
(8) Yi, G.-R.; Thorsen, T.; Manoharan, V. N.; Hwang, M.-H.; Jeon, S.-J.; Pine, D. J.; Quake, S. R.; Yang, S.-M. *Adv. Mater.* **2003**, *15*, 1300−1304.
(9) Shepherd, R. F.; Conrad, J.; Rhodes, S.; Marquez, M.; Weitz, D.A.; Lewis, J. A. *Langmuir* **2006**, *22*, 8616−8622.
(10) Walls, H. J.; Caines, S. B.; Sanchez, A. M.; Khan, S. A. S. *J. Rheol.* **2003**, *47*, 847−868.
(11) Haw, M. D. *Phys. Rev. Lett.* **2004**, *92*, 185506-1−185506-4.
(12) Hunter, R. J.; Friend, R. H. *J. Colloid Interface Sci.* **1971**, *37*, 548−556.
(13) Hunter, R. J.; Frayne, J. *J. Colloid Interface Sci.* **1980**, *28*, 107−115.
(14) Bingham, E. C. *Bur. Stand. (U.S.), Bull.* **1916**, *13*, 309−353.
(15) Bulkley, W. H.; Herschel, A. R. *Kolloid−Z.* **1926**, *39*, 291−300.
(16) Bird, R. B.; Dai, G. C.; Yarusso, B. J. *Rev. Chem. Eng.* **1983**, *1*, 1−67.
(17) Alexandrou, A. N.; McGilvreay, T. M.; Burgos, G. *J. Non-Newtonian Fluid Mech.* **2001**, *100*, 77−96.
(18) Burgos, G. R.; Alexandrou, A. N. *J. Rheol.* **1999**, *43*, 463−483.
(19) Sayed-Ahmed, M. E. *Int. Commun. Heat Mass Transfer* **2000**, *27*, 1013−1024.
(20) Santiago, J. G.; Wereley, S. T.; Meinhart, C. D.; Beebe, D. J.; Adrian, R. J. *Exp. Fluids* **1998**, *25*, 316−319.
(21) Meinhart, C. D.; Wereley, S. T.; Santiago, J. G. *Exp. Fluids* **1999**, *27*, 414−419.
(22) Frank, M.; Anderson, D.; Weeks, E. R.; Morris, J. F. *J. Fluid Mech.* **2003**, *493*, 363−378.
(23) Gotz, J.; Buggisch, H. *J. Non-Newtonian Fluid Mech.* **1993**, *49*, 251−275.

10.1021/la700562m CCC: $37.00
Published on Web 07/13/2007

material are acquired. Instantaneous velocity fields are then obtained by cross-correlation of the images, from which the flow profile is determined.[20,21,24] Our experimental system consists of hydrophobically modified silica microspheres suspended in a polar index-matching medium, which contains a small population of fluorescent tracers. We observe a transition from plug flow to a profile more consistent with that of a colloidal fluid as the flow rate is increased. We hypothesize that this behavior is the result of a transition from unyielded flow dominated by wall slip to flow of a ruptured gel network. Moreover, we show by direct measurements of the flow velocity that the commonly used Herschel−Bulkley model fails to capture the behavior of our system at large $\dot{\gamma}$. Rather, a modified power-law model that accounts for its finite viscosity at large $\dot{\gamma}$ more accurately predicts the observed flow profiles.

Experimental Methods

Materials System. Silica microspheres (lot #AN3316, Fuso Chemical, Osaka, Japan) with a mean diameter of 493 nm, a specific surface area of 6.91 m^2/g, and a density of 2.24 g/cm^3, as measured by transmission electron microscopy (CM-12, Phillips, Eindhoven, The Netherlands), nitrogen adsorption (Autosorb 1-Series, Quantachrome, Boynton Beach, FL), and helium pycnometry (model 1330, Micromeritics, Norcross, GA), respectively, are used in all experiments. Stable colloidal fluids are produced by suspending bare silica particles ($\phi = 0.21$) in a 4:1 (w/w) mixture of dimethylsulfoxide (DMSO) and water, to which potassium hydroxide is added at a concentration of 10^{-4} M to induce an appropriate surface charge on these species. Flocculated colloidal gels are produced by rendering the silica microsphere surface partially hydrophobic by reacting it with an organosilane coupling agent.[25,26] Specifically, we reacted chloro(dimethyl octylsilane) (Fluka Chemical, St. Louis, MO) with silica microspheres suspended in toluene (Aldrich Chemical, St. Louis, MO). This coupling agent is added in 10 separate aliquots to ensure uniform surface coverage. Triethylamine (Aldrich Chemical) is also added at a ratio of 2 μL of triethylamine to 1 μL of organosilane (molar ratio of 3.4:1) as an acid scavenger. The reaction mixture is stirred for 24 h under low heat. The particles are then dried, resuspended in acetone, filtered through a 20 μm mesh nylon filter (Small Parts, Miami Lakes, FL) to eliminate any permanent aggregates, and dried a second time before use.

Colloidal gels ($\phi = 0.15-0.33$) are prepared by mixing the appropriate amounts of dried silica particles with a refractive index matching mixture of DMSO (Aldrich Chemical) and deionized water at a ratio of 4:1 (w/w). The particles are added in three separate aliquots, and the suspension is sonicated after each addition (Fisher Scientific, model 500) for 30 s in a 1 s on/1 s off pulse sequence. The sample is then sonicated a final time for 3.5 min in a 1 s on/1 s off pulse sequence. An appropriate amount of fluorescent polystyrene microspheres (1 μm in diameter, Nile Red, Invitrogen, Carlsbad, CA) are then added to achieve a final volume fraction of $\phi_{PS} = 6 \times 10^{-4}$, which is necessary to optimize the image quality for μPIV. Direct visualization of samples by confocal microscopy (SP2, Leica, Wetzlar, Germany) confirms that the tracers are incorporated within the colloidal gel network (data not shown). The final colloid volume fraction in each suspension is verified by weighing a representative sample before and after solvent removal at elevated temperatures.

Rheological Measurements. Rotational and oscillatory measurements are carried out using a controlled stress rheometer (CVOR, Malvern Instruments, Southborough, MA). For rotational viscometry, three different measuring geometries are used. A 25 mm double-gap measuring system is used at $\phi = 0.15$ to ensure a measurable torque. Concentric cylinders with splined fixtures (15.4 mm cup and 14 mm bob) are used, when $\phi = 0.20$. At higher colloid volume fractions ($\phi = 0.25-0.33$), a six-bladed vane tool (14 mm) in a splined 15.4 mm cup is used, since more concentrated colloidal gels exhibit wall slip in the roughened concentric cylinder geometry (data not shown). To minimize the effects of shear history on the rheological data, each sample is sonicated for 30 s in a 1 s on/1 s off pulse sequence and allowed a 1 h quiescent period prior to each experiment. The apparent viscosity is measured over the range of shear rates, 0.001 $s^{-1} < \dot{\gamma} < 100\ s^{-1}$. For oscillatory measurements, a six-bladed vane tool is used in a splined 14 mm cup with a gap size of 0.7 mm. The elastic (G') and viscous (G'') moduli are measured over the range of stresses, 0.01 Pa $< \tau <$ 100 Pa, at a frequency of 1 Hz and a strain of approximately 10^{-4}.

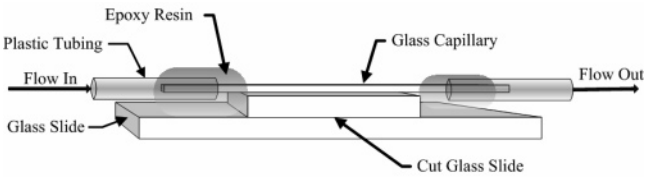

Figure 1. Flow cell used in μPIV measurements. Colloidal suspensions flow through the square glass capillary tube, where images are collected.

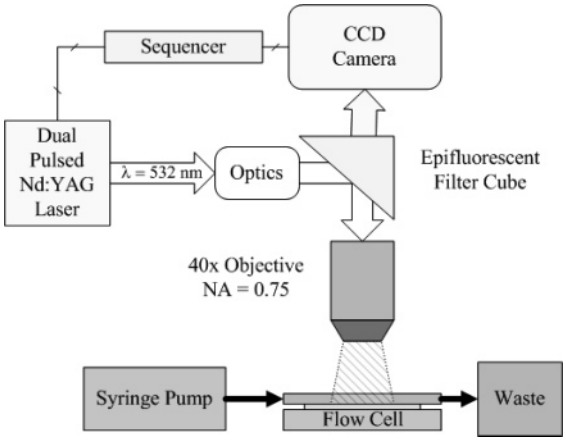

Figure 2. Experimental apparatus for μPIV experiments. A pulsed laser system is used for illumination, and images are acquired by a CCD camera through an epifluorescence microscope. The camera and laser system are coordinated by means of a synchronizer that is controlled by a PC. Flow through the flow cell is provided by a syringe pump.

Microscopic Particle Image Velocimetry. The flow cell utilized in this work is similar to that used previously[21,22] and is shown in Figure 1. A 100 × 100 μm^2 square polyimide capillary tube (Polymicro, Phoenix, AZ) is first prepared by cutting a 40 mm length of square tubing and removing the polyimide coating by heat. The capillary tube is then attached to a 25 × 25 mm^2 glass microscope slide (Fisher Scientific) by means of a quick-cure epoxy resin (Devcon). This assembly is bonded to a 75 × 25 × 1 mm^3 microscope slide using this epoxy. A 200 mm length of 28 gauge Teflon tubing is then affixed to the glass capillary at either end by inserting the capillary into the Teflon tubing and sealing the assembly with epoxy. During testing, sample flow is controlled by a syringe pump (Harvard Apparatus, Holliston, MA).

The imaging apparatus utilized in this work is similar to that used by Meinhart et al.,[21] and is shown in Figure 2. Flow is imaged through an epifluorescence microscope (Olympus BX60, Olympus, Center Valley, PA) with a 40× objective (N.A. = 0.5). Illumination is provided by a pulsed Nd:YAG laser system ($\lambda = 532$ nm). A set of high- and low-pass filters in series is used to ensure proper excitation, direct the beam, and isolate the emitted light from the excitation source prior to imaging the tracer particles. Images are collected by a 12-bit cooled, frame-straddle CCD camera (PIVCAM 13-10, TSI, Shoreview, MN) with a resolution of 1280 × 1024 pixels. The timing of the laser pulses is adjusted to facilitate the acquisition of image pairs with a minimum time separation of 1 μs

(24) Adrian, R. J. *Annu. Rev. Fluid Mech.* **1991**, *23*, 261−304.
(25) Xu, Z.; Yoon, R.-H. *J. Colloid Interface Sci.* **1989**, *132*, 532−441.
(26) Xu, Z.; Yoon, R.-H. *J. Colloid Interface Sci.* **1990**, *134*, 427−434.

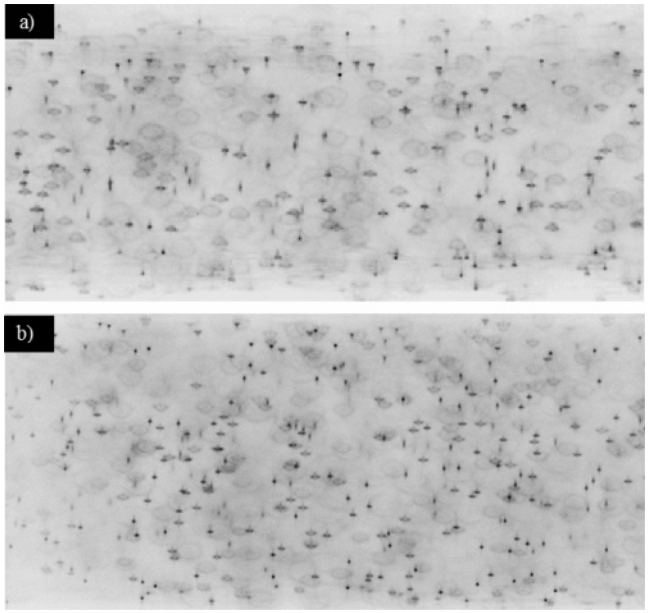

Figure 3. Images taken for μPIV analysis of (a) a dilute suspension of tracers in deionized water and (b) a stable colloidal suspension ($\phi = 0.21$) containing tracers. In both images, the tracer particles are clearly visible, demonstrating that the refractive indices of the colloidal particles and the suspending medium are sufficiently close. The images are inverted to allow for visual clarity.

at a maximum rate of 3.75 Hz. An electronic synchronizer (Laserpulse 610034, TSI) that controls the timing of illumination and image acquisition is regulated by a commercially available software package (Insight 3.2, TSI, Shoreview, MN). For all experiments, the timing between image pairs is adjusted to obtain a maximum particle displacement of 10−12 pixels, thereby reducing the relative velocity measurement errors to approximately 1%.[27,28] On the basis of studies of flowing tracer suspensions in deionized water, the expected error in the velocity is 5−7%. This error arises primarily due to fluctuations in flow that stem from the syringe pump.

Images are acquired over a range of volume fractions ($\phi = 0.15-0.33$) and flow rates ($Q = 1-50$ μL/min), which correspond to maximum shear rates in excess of 1000 s^{-1}. These measurements are made downstream at a location of 20 mm, ensuring fully developed laminar flow, and at the depth-wise midplane of the channel cross-section where the near-zero out-of-plane velocity gradients ensure minimal depth averaging effects due to the finite depth of focus of the imaging system (~ 5 μm). When the desired flow rate is achieved, an ensemble of 100 sequential image pairs is collected. These image pairs are interrogated using the commercial software package described above to obtain an instantaneous vector field for each image pair in the ensemble.[20,24,27,28]

The resulting vector fields are then validated by means of a freely available software package (CleanVec, Laboratory for Turbulence and Complex Flow, University of Illinois) that removes erroneous vectors via objective statistical comparisons. Holes generated by this removal procedure are filled with interpolated values when more than half of the nearest neighbors are present. Each vector field is then spatially filtered to remove high-frequency noise. Following validation, all vector fields in an ensemble are averaged, and the velocity is computed based on the pixel displacement and the time between images in an image pair. The dimensionless velocity, U/U_{max}, is then calculated where U is the velocity in the direction of flow and U_{max} is the maximum value of U across the channel. The dimensionless velocity is then plotted in terms of the dimensionless position, x/L, where x is the distance from the tube center in the direction perpendicular to the microchannel axis and L represents half of the width of the microchannel.

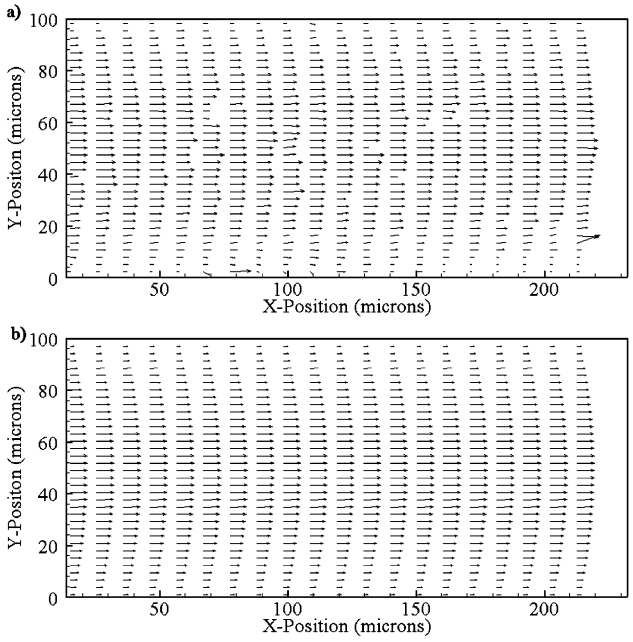

Figure 4. Sample vector fields for a stable colloidal fluid, $\phi = 0.21$, $Q = 50$ μL/min. Ensembles of 100 individual vector fields (a) are validated and averaged to produce the final result (b).

Scattering from colloidal particles in a concentrated suspension can impair the image quality in the μPIV experiments. To ensure that scattering does not significantly affect the quality of data obtained by μPIV, preliminary tests are carried out on a stable colloidal fluid composed of bare silica particles ($\phi = 0.21$) suspended in a 10^{-4} M solution of potassium hydroxide in a 4:1 (w/w) mixture of DMSO and water. As shown in Figure 3, images obtained for this suspension are comparable in quality to those obtained for a dilute suspension of fluorescent tracers in deionized water. The images yield raw vector fields that are validated and averaged as described above (see Figure 4a,b). This finding confirms that the system is sufficiently index-matched such that scattering effects are minimized.

The experimentally measured velocity profiles for the stable colloidal fluid at various flow rates are shown in Figure 5a. Each profile exhibits parabolic behavior, as expected for a Newtonian fluid based on a solution of the Navier−Stokes equations.[29,30] Similar agreement is observed when the measured maximum velocities are compared with theoretical predictions for a Newtonian fluid at various flow rates, as shown in Figure 5b. However, near the channel walls, the observed flow profiles deviate slightly from the expected Newtonian behavior due to the modest shear thinning behavior of the suspension. Such deviations have also been observed by confocal microscopy carried out on flowing hard-sphere suspensions.[22]

Finite-Element Modeling. For unidirectional flow in rectilinear geometry, the momentum balance equation reduces to the following form:[31−33]

$$\frac{\partial p}{\partial z} = \frac{\partial}{\partial y}\left(\eta \frac{\partial U}{\partial y}\right) + \frac{\partial}{\partial x}\left(\eta \frac{\partial U}{\partial x}\right) \quad (2)$$

where η is the viscosity, p is the pressure, z is the axial direction of flow, and U is the fluid velocity in the z-direction. For non-Newtonian fluids, where $\eta = f(\dot{\gamma})$, eq 2 can generally be solved by the finite-element method (FEM).[17−19,33] We use a commercially available software package (COMSOL Multiphysics, COMSOL,

(27) Keane, R. D.; Adrian, R. J. *Meas. Sci. Technol.* **1990**, *1*, 1202−1215.
(28) Keane, R. D.; Adrian, R. J. *Meas. Sci. Technol.* **1990**, *2*, 963−974.
(29) Habdas, P.; Weeks, E. R. *Curr. Opin. Colloid Interface Sci.* **2002**, *7*, 196−203.
(30) Shah, R. K.; London, A. L. *Laminar Flow Forced Convection in Ducts: A Source Book for Compact Heat Exchanger Analytical Data*; Academic Press: New York, 1978.
(31) Panton, R. L. *Incompressible Flow*; Wiley: New York, 1996.
(32) Batchelor, G. K. *An Introduction to Fluid Dynamics*; Cambridge University Press: Cambridge, U.K., 2000.
(33) Syrjala, S. *Int. Commun. Heat Mass Transfer* **1995**, *22*, 54−557.

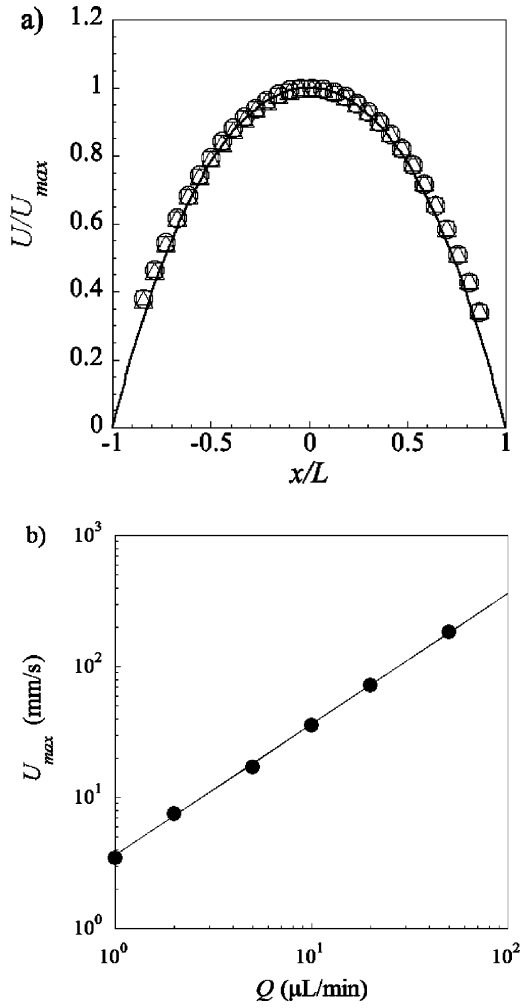

Figure 5. (a) Dimensionless velocity (U/U_{max}) as a function of dimensionless tube position (x/L) for the colloidal fluid ($\phi = 0.21$): $Q = 1$ (open circles), 10 (open triangles), and 50 (open squares) μL/min. Symbols correspond to experimental data, whereas the solid line indicates the dimensionless solution for laminar flow in a square capillary tube. (b) Maximum velocity for the colloidal fluid as a function of flow rate. Symbols correspond to experimental results, whereas the solid line indicates the solution of the Navier−Stokes equation for a Newtonian fluid.

Burlington, MA) to predict flow profiles for our model gel system in square channels. One-quarter of the channel's cross-section is modeled subject to symmetry boundary conditions in the tube center and no-slip conditions at the walls. We express η as a function of $\dot{\gamma}$ by means of an empirical model based on viscometry data. The finite-element solution is then compared to the normalized velocity profile from μPIV experiments.

Results and Discussion

Viscoelastic Behavior of Colloidal Gels. The apparent viscosity, η, is plotted as a function of the applied shear rate, $\dot{\gamma}$, in Figure 6a for colloidal gels of varying volume fraction ($0.15 \leq \phi \leq 0.33$). Each suspension exhibits marked shear-thinning behavior with η increasing dramatically as ϕ increases at constant $\dot{\gamma}$. In Figure 6b, the gel elastic modulus, G', is plotted as a function of the applied stress, τ. Within the linear viscoelastic region, a well-defined equilibrium modulus, G_0', is observed. At higher τ, the value of G' declines sharply due to yielding and breakup of the gel network, which leads to the onset of fluid-like behavior. We define the yield stress τ_y from the data shown in Figure 6b, as the value of τ_y where $G' = 0.9G_0'$.[4] We find that both G_0' and τ_y exhibit a power-law dependence on ϕ, where $G_0' = 3.3 \times 10^5\phi^{3.7}$ and $\tau_y = 43\phi^{2.7}$, and G_0' and τ_y have units of Pa. Our observations are in good accord with prior studies of colloidal gels produced by alternate gelation mechanisms.[3−5]

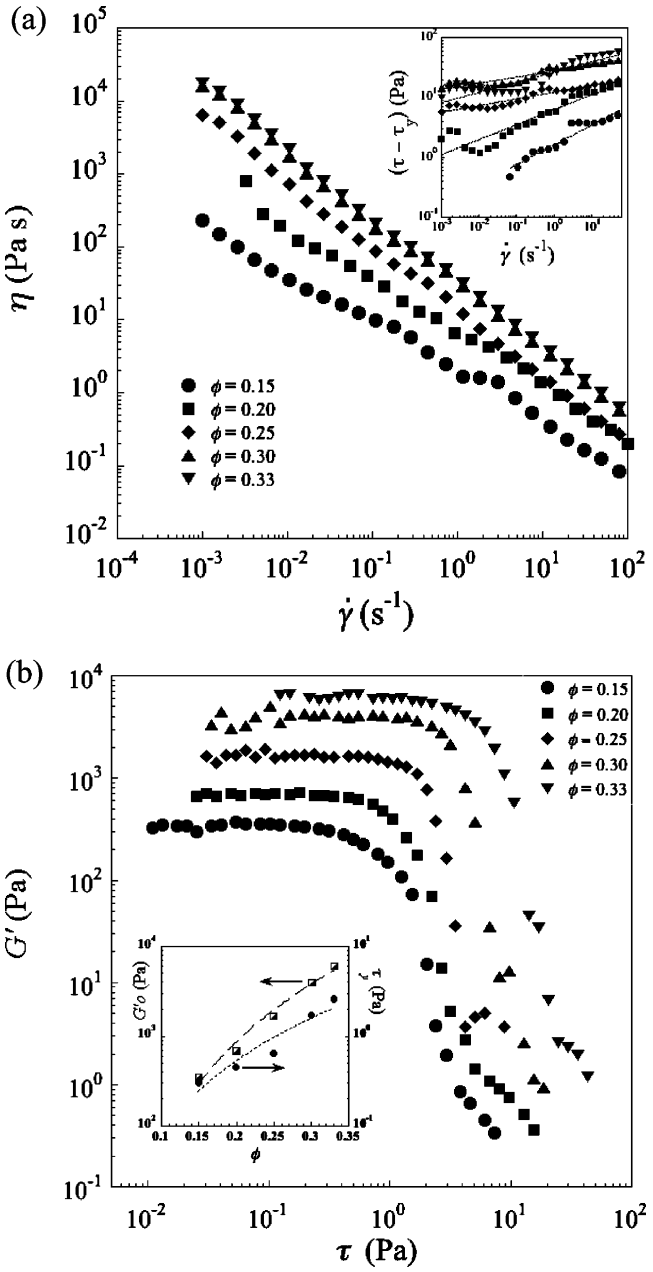

Figure 6. (a) Apparent viscosity as a function of shear rate for model colloidal gels of varying ϕ. The plot used to fit the viscosity data to the Herschel−Bulkley model is shown in the inset. (b) Elastic modulus (G') as a function of shear stress (τ) for a colloidal gel system at varying ϕ. Oscillatory measurements are conducted at a frequency of 1 Hz. The inset shows the plateau modulus and yield stress as a function of colloid volume fraction, where the dashed lines show a two-parameter power-law fit to the data.

The shear rheology of colloidal gels is often described by the Herschel−Bulkley model.[4,14−16] To extract the parameters K and n from the rheological measurements, we plot $\tau - \tau_y$ versus $\dot{\gamma}$ in the inset of Figure 6a. A power-law fit with two adjustable parameters yields K and n for each data set. These parameters are plotted as a function of ϕ in Figure 7 and show the following empirical relationships: $K = 1540\phi^{3.5}$ and $n = 0.028\phi^{-1.3}$, where K has units of Pa·s^{-n} and n is dimensionless. Below, we compare

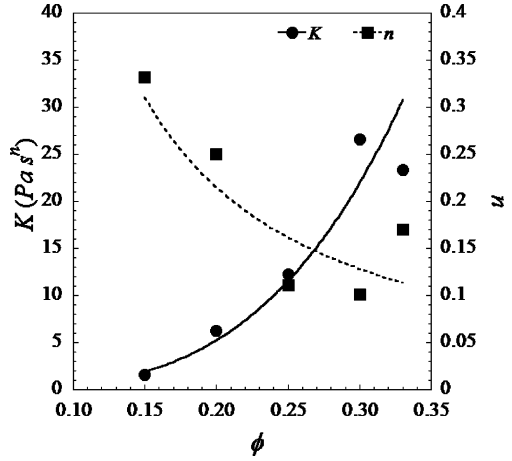

Figure 7. Plot of parameters for the Herschel−Bulkley model for the colloidal gel system. The parameters K and n are plotted as a function of colloid volume fraction, along with the fits given by $K = 1540\phi^{3.5}$ (solid line) and $n = 0.028\phi^{-1.3}$ (dashed line).

the flow profiles of these colloidal gels in square microchannels observed experimentally to those predicted by this rheological model.

Microparticle Image Velocimetry of Colloidal Gels in Microchannels. The flow profiles of colloidal gels in square microchannels measured at various values of Q and ϕ are shown in Figure 8. For brevity, we only report data for three of the five ϕ values investigated. Each flow profile is normalized by its corresponding maximum velocity, U_{max}, and plotted against the dimensionless position in the microchannel, x/L, where x is the distance from the tube center and L represents the microchannel half-width. We observe a qualitative change in the shape of the flow profile as Q increases. At low Q, U/U_{max} is constant across a large fraction of the microchannel, indicative of behavior similar to plug flow. We define the dimensionless plug width, α, as the fraction of the channel width over which $U > 0.95U_{max}$. In Figure 9, α is plotted as a function of Q for various ϕ. Only values of $x/L \leq 0.8$ are utilized to determine α due to the availability of limited data at higher x/L (see Figure 8). Hence, the maximum α values reported in Figure 9 represent the minimum plug width for a given volumetric flow rate. We find that there is a monotonic decrease in α with increasing Q, which reflects a steady transition to more fluid-like behavior. This trend is observed for all values of ϕ, but is more pronounced at low ϕ. To better illustrate this transition, we show the experimentally measured U_{max} as a function of Q in Figure 10. Two limiting cases are also plotted: the average velocity, U_{avg}, and the maximum velocity expected for a Newtonian fluid, $U_{max,N}$. Note, if plug flow occurs across the entire channel, we would expect $U_{max} = U_{avg}$. As Q increases, we observe a transition in U_{max} from values close to U_{avg} to those approaching $U_{max,N}$, indeed confirming the transition from plug flow to more fluid-like behavior. This transition occurs when the shear stress within the microchannel exceeds the measured yield stress (τ_y) of the colloidal gel. To our knowledge, direct observations of the yielding transition and its correlation with bulk rheological measurements have not been previously reported for colloidal gels.

Finite-Element Modeling of Colloidal Gels in Microchannels. We first compare our experimental results to FEM predictions of the dimensionless flow profiles based on the Herschel−Bulkley model, where the gel viscosity is given by $\eta = \tau_y/\dot{\gamma} + K\dot{\gamma}^{n-1}$. As shown in Figure 8, these predicted flow profiles deviate substantially from the experimentally observed behavior, especially at $Q \leq 2$ μL/min and $Q \geq 10$ μL/min. For $Q \leq 2$ μL/min, the measured flow profile is flat across a larger portion of the channel, that is, the behavior is more similar to plug-flow, than predicted by the model. We attribute this deviation to slip at the microchannel walls, which typically arises due to a thin fluid layer between the flowing gel and the nozzle wall.[4,10,31] For $Q \geq 10$ μL/min, the model does not predict the observed transition to more fluid-like behavior with increasing Q.

As the above comparison illustrates, the Herschel−Bulkley model fails to adequately capture the experimentally observed behavior. This model predicts that $\eta \rightarrow 0$ as $\dot{\gamma} \rightarrow \infty$, which is physically unrealistic for colloidal gels. The apparent viscosity is therefore effectively reduced to a two-parameter power-law form, since $\tau_y/\dot{\gamma} \ll K\dot{\gamma}^{n-1}$ for the values of $\dot{\gamma}$, τ_y, K, and n relevant

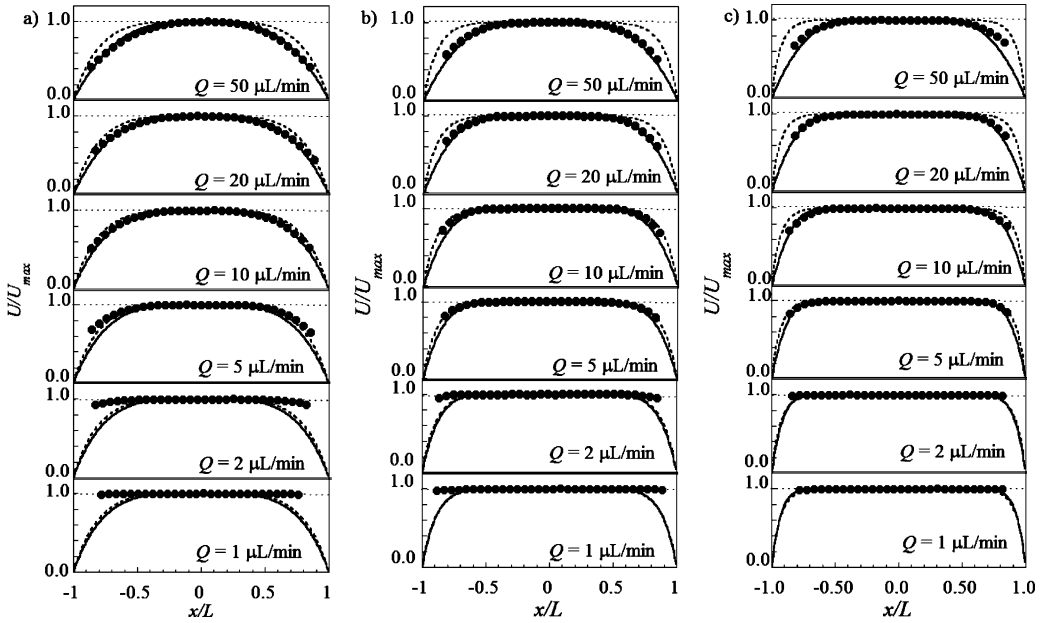

Figure 8. Plot of dimensionless velocity (U/U_{max}) as a function of dimensionless tube position (x/L) for colloidal gels at (a) $\phi = 0.15$, (b) $\phi = 0.24$, and (c) $\phi = 0.33$. [Note: In these plots, the experimental data (filled circles) are compared to predictions made by the Herschel−Bulkley model (bold dashed line) and a modified rheological model that accounts for the finite viscosity of the gel at infinite shear (solid line).]

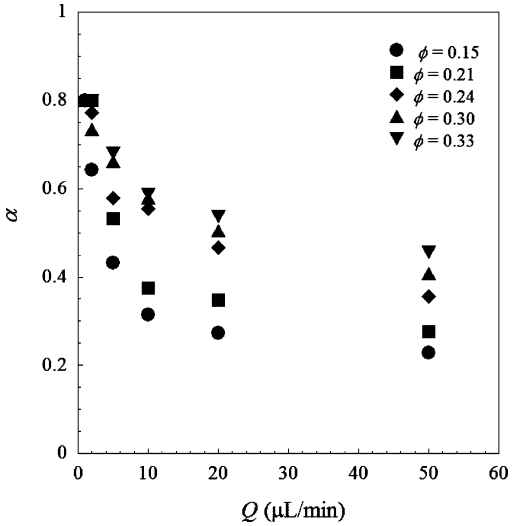

Figure 9. Plot of dimensionless plug width (α) as a function of volumetric flow rate (Q) for colloidal gels of varying ϕ. [Note: α is calculated using data in the range $|x/L| \leq 0.8$. Hence, the reported values represent a minimum estimate of the plug width.]

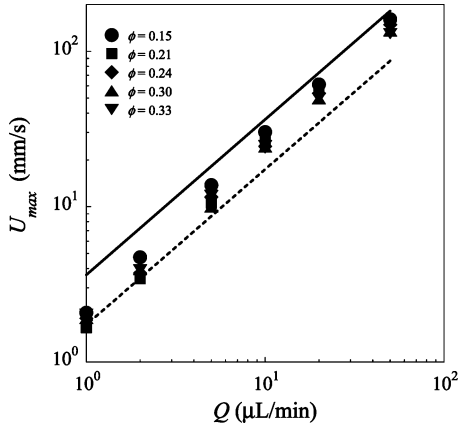

Figure 10. Log−log plot of U_{max} as a function of volumetric flow rate (Q) for colloidal gels of varying ϕ. Theoretical values of U_{max} (solid line) and U_{avg} (dashed line) are plotted for reference.

to our experimental system. For these conditions, the calculated normalized flow profiles are found to be invariant with respect to Q.

To correct this, the proper high-shear behavior of colloidal gels must be taken into account. At high $\dot{\gamma}$, the gel microstructure is broken into small clusters in the suspending medium.[12,13] Because the sheared network possesses a finite viscosity under these conditions, we replace $\tau_y/\dot{\gamma}$ with the simplest term that will remain finite as $\dot{\gamma} \rightarrow \infty$. At high $\dot{\gamma}$, we assume that this system behaves similarly to that of a dispersed suspension, whose apparent viscosity is given by the Krieger−Dougherty relationship:[34]

$$\eta_\infty = \eta_s\left(1 - \frac{\phi}{\phi_m}\right)^{-[\eta]\phi_m} \quad (3)$$

where ϕ_m is the colloid volume fraction at maximum packing, $[\eta]$ is the intrinsic viscosity, and η_s is the viscosity of the suspending medium. The term η_∞ represents the suspension viscosity at infinite shear. We choose $\phi_m = 0.68$ and $[\eta] = 2.5$ on the basis of prior studies of hard-sphere suspensions under high shear conditions.[34,35] The gel viscosity is now given by

$$\eta = \eta_\infty + \kappa\dot{\gamma}^{\nu-1} \quad (4)$$

where κ represents the power-law viscosity, and ν is the shear-thinning exponent. This expression is similar to that first used by Sisko in the study of lubricating greases.[36]

To determine κ and ν from rheological data, we plot $\eta - \eta_\infty$ as a function of $\dot{\gamma}$ based on the experimental measurements shown in Figure 6b. A two-parameter power-law fit to $\eta - \eta_\infty$ yields κ and ν at each ϕ. The data (not shown) are best described by the following empirical power-law relationships: $\kappa = 2200\phi^{3.7}$ and $\nu = 1.1 \times 10^{-2}\phi^{-1.8}$, where κ has units of Pa·s$^{-\nu}$ and ν is dimensionless. The flow profiles calculated using this new model are depicted by solid lines in Figure 8. These predictions exhibit much better agreement with our experimental findings than the commonly used Herschel−Bulkley model, particularly when $Q \geq 10$ μL/min, that is, under conditions where the colloidal gels experience high shear rates within the square microchannels. Hence, our results demonstrate that the finite gel viscosity at large $\dot{\gamma}$ must be taken into account to properly predict the flow behavior of these systems in confined geometries.

Conclusions

We directly measured the flow profiles of colloidal gels of varying volume fraction in square microchannels by μPIV. We observed a transition from plug flow to more fluid-like behavior as Q increased. This transition is not captured by the Herschel−Bulkley model, which predicts a flow profile that is independent of Q for the range of parameters obtained from rheological measurements. When $Q > 10$ μL/min, we show that the failure of the Herschel−Bulkley model stems from its prediction that $\eta \rightarrow 0$ as $\dot{\gamma} \rightarrow \infty$, which is physically unrealistic for colloidal gels. To correct this, we apply a rheological model that accounts for power-law shear thinning and the finite viscosity of the colloidal gel at high shear rates. The flow profiles obtained on the basis of this relationship show better agreement with our experimental results, particularly at higher values of Q. Our results offer new insight into the flow behavior of colloidal gels in confined geometries, and, thus, have important implications on microfluidic, extrusion, and direct ink writing approaches that rely on these materials as feedstock for materials assembly.

Acknowledgment. The authors gratefully acknowledge the generous funding for this project provided by the NSF Center for Nanoscale Chemical-Electrical-Mechanical Manufacturing Systems (Grant# DMII -0328162) and the NSF Center for Directed Assembly of Nanostructures (Grant# DMR01-17792). We thank R. Shepherd for preparing the Table of Contents image.

LA700562M

(34) Krieger, I. M. *Adv. Colloid Interface Sci.* **1972**, *3*, 111−136.
(35) Choi, G. N.; Krieger, I. M. *J. Colloid Interface Sci.* **1986**, *113*, 101−112.
(36) Sisko, A. W. *Ind. Eng. Chem.* **1958**, *50*, 1789−1792.